Articles in PresS. J Neurophysiol (November 8, 2017). doi:10.1152/jn.00371.2017

Optimal use of limb mechanics distributes control during bimanual tasks

Abbreviated title: Optimal use of biomechanics during bimanual control

Authors:

Córdova Bulens D. [1,2], Crevecoeur F. [1,2], Thonnard J-L. [1,3], Lefèvre P. [1,2]

Affiliations :

[1] Institute of Neuroscience (IoNS), Université catholique de Louvain, 1050 Brussels, Belgium.

[2] Institute of Information and Communication Technologies, Electronics and Applied Mathematics (ICTEAM), Université catholique de Louvain, 1348 Louvain-la-Neuve, Belgium.

[3] Physical and Rehabilitation Medicine Department, Cliniques Universitaires Saint-Luc, 1050 Brussels, Belgium.

Corresponding author:
P. Lefèvre,
4 Avenue Georges Lemaître
1348 Louvain-la-Neuve, Belgium
Tel. : +3210472382
philippe.lefevre@uclouvain.be

Abstract

Bimanual tasks involve the coordination of both arms, which often offers redundancy in the ways a task can be completed. The distribution of control across limbs is often considered from the perspective of handedness. In this context, although there are differences across dominant and non-dominant arms during reaching control (Sainburg 2002), previous studies have shown that the brain tends to favor the dominant arm when performing bimanual tasks (Salimpour and Shadmehr 2014). However, biomechanical factors known to influence planning and control in unimanual tasks may also generate limb asymmetries in force generation, but their influence on bimanual control has remained unexplored. We investigated this issue in a series of experiments in which participants were instructed to generate a 20-N force with both arms, with or without perturbation of the target force during the trial. We modeled the task in the framework of optimal feedback control of a two-link model with six human-like muscles groups. The biomechanical model predicted a differential contribution of each arm dependent on the orientation of the target force and joint configuration that was quantitatively matched by the participants' behavior, regardless of handedness. Responses to visual perturbations were strongly influenced by the perturbation direction, such that online corrections also reflected an optimal use of limb biomechanics. These results show that the nervous system takes biomechanical constraints into account when optimizing the distribution of forces generated across limbs during both movement planning and feedback control of a bimanual task.

New & Noteworthy

Here, we studied a bimanual force production task to examine the effects of biomechanical constraints on the distribution of control across limbs. Our findings show that the central nervous system optimizes the distribution of force across the two arms according to the joint configuration of the upper-limbs. We further show that the underlying mechanisms influence both movement planning and online corrective responses to sudden changes in the target force.

Introduction

Generally, healthy people are able to perform a wide variety of tasks that require the coordination of several actuators. For instance, steering an automobile involves a coordinated effort of two arms, but the effort produced can be distributed across the arms in a variety of ways. During the performance of bimanual tasks, the central nervous system (CNS) must deal with redundancy and share control across limbs. An important factor to consider in this sharing is the asymmetry across flexor and extensor muscles (Kawakami et al. 1994), which may favor an anisotropic contribution of each arm during bimanual actions.

To date, the main source of limb-use asymmetry that has been considered is hand dominance. Previous studies have shown that the CNS favors the dominant hand during bimanual tasks (Swinnen et al. 1996; Salimpour and Shadmehr 2014; Salimpour et al. 2015). Generally, this tendency is attributed to the lesser variability that is associated with controlling the dominant arm (Kalisch et al. 2006), which may, in principle, impact how the brain coordinates the two arms in bimanual tasks (O'Sullivan et al. 2009). Compatible with this hypothesis, Salimpour and Shadmehr (2014) reported that the dominant arm showed less variability during unimanual force production and suggested that this limb contributed more during a bimanual force-production task.

Beyond handedness, the possibility that biomechanical properties influence how we distribute control across our limbs has remained largely unexplored. However, in the context of unimanual tasks, it is clear that the CNS monitors biomechanical constraints arising during movements and adjusts subsequent motor decisions or trajectories accordingly (Sabes et al. 1998; Cos et al. 2011, 2012, 2013). It has been established that the CNS accounts for torque interactions at the shoulder and elbow joints during planning and control of reaching movements (Hollerbach and Flash 1982; Gribble and Ostry 1999; Dounskaia et al. 2011, 2014; Wang et al. 2012). Other parameters such as expected effort and success affect the arm choice when performing reaching movements

(Schweighofer et al. 2015). Given the strong influence of biomechanics on unimanual control, we hypothesized that biomechanical factors should also play an important role in bimanual control.

To test this hypothesis, we adopted an isometric force production paradigm for two limbs (Salimpour and Shadmehr 2014) and modified it for variance of the orientation of target forces and joint configurations to asses how biomechanical factors influence the contribution of each arm to overall force generation during both motor planning and online corrective responses. We developed an optimized control model of two human-inspired two-jointed arms with which to predict optimal cooperation of the arms across three different joint configurations. We tested how well the model could predict the way right- and left-handed human participants distribute force across their arms. The model accounts for optimization of weighting of each limb during both unperturbed movements and responses to perturbations with visual feedback and was used to predict the influence of biomechanics on the force distribution across arms. We predicted that the arms' joint configuration would be shown to have a strong influence on the participants' adjustments to the distribution of forces produced across the limbs.

Materials and Methods

Participants

Ten healthy right-handed participants (6 females, average Oldfield score 95, 9th right decile) and ten healthy left-handed participants (5 females, average Oldfield score -88.5, 7th left decile) participated in Experiment 1. Twelve right-handed participants (4 females, average Oldfield score 90, 7th right decile) participated in Experiment 2. The average age of participants was 27 years old. All participants provided written informed consent before participating in this study. The volunteers had no known neurological disorders and were naïve to the purpose of the experiment. Handedness was assessed using the Edinburgh Inventory (Oldfield 1971). The experimental procedures were approved by the local ethics committee at the *Université catholique de Louvain*.

Behavioral task

Two different experiments were performed using the same general paradigm. Participants held the handles of two robotic arms (KINARM, BKIN Technologies, Kingston), one in each hand (Fig. 1A). Each handle was equipped with a force sensor (Mini-40 F/T sensors, ATI Industrial Automation, NC, USA). The forces measured by the transducers were mapped onto cursor position on a virtual reality display. Direct vision of the limbs and of the robotic handles was blocked. The robotic arms counteracted the forces applied by the subject with a very stiff force field (K = 2000 N/m, B = 50 N·s/m). This force field limited movement of the robotic and participants' arms to negligible movements (isometric task). The position of the cursor (radius, 0.5 cm), which was denoted by the two-dimensional vector $\vec{z}$, was proportional to the sum of the force vectors $\overrightarrow{f_L}$ and $\overrightarrow{f_R}$ produced by the left and right arm, respectively (see Fig. 1A):

$$\vec{z} = b\left(\overrightarrow{f_L} + \overrightarrow{f_R}\right) + \overrightarrow{z_0} \qquad (1)$$

In eq. (1), $\overrightarrow{z_0}$ is the center of the workspace, corresponding to the initial location of the cursor with no forces being applied to the handles. The scaling factor b was set to 0.5 cm/N. At the beginning of each trial, a reference target (radius 1 cm) was displayed at the center of the workspace. After 1 s, the reference target vanished and a goal target appeared in one of 16 possible positions equally spaced around a circle with a 10-cm radius, centered on the reference target site (see Fig. 1C). The goal of the task was to produce a total force of 20 N in the direction of the target. Participants were instructed to reach the target within 800 ms, and then to maintain the cursor at the target site for 1 s. Participants were instructed to perform the task using both arms at the same time. Trials in which the ratio of forces produced by the two arms exceeded 10:1 were considered to be unimanual trials and omitted (5.75% of all trials were omitted; participant trial omission range, 0–27%). Participants' arms were supported against gravity in the horizontal plane by slings, arm joint configurations were described in terms of elbow and shoulder joint angles (θ_1 and θ_2, respectively, in Fig. 1B).

In experiment 1, three different joint configurations were tested in three configuration-specified blocks (Fig. 2A). Joint angles were measured by a goniometer at the start of each block; the means and standard deviations of the measured joint angles for each configuration are reported in Table 1. In each configuration, the 16 possible targets were presented in a random order with each target being presented 10 times, resulting in 160 trials per configuration and a total of 480 trials for each subject.

In experiment 2, the subjects performed the task with their arms constrained to configuration 3 (Fig. 2A) with eight possible targets (Fig. 2C, red circles). In 80% of the trials, the cursor relocated perpendicular relative to the target direction midway through the movement (Fig. 1D). The relocated cursor appeared 3 cm or 5 cm, clockwise (CW) or counterclockwise (CCW), from the cursor's last location. We employed an orthonormal definition of location relative to initial reach direction such that cursor relocations in the CW and CCW direction were termed negative and positive cursor jumps, respectively. The presentation of these four possible cursor jump amplitudes (-5 cm, -3 cm, -5 cm, and +5 cm) and the unperturbed condition (0 cm, 20% of trials) was random in order, but balanced in quantity for each subject. To reach the target, subjects had to adapt the forces they were applying to correct for the cursor's shift in location which allowed us to study whether biomechanics has an influence on corrective online responses or not. More precisely, if online corrections use the same weighting as during the planning phase then we should observe no change in the force distribution across limbs following a cursor jump, leading to the same force distribution across arms as during unperturbed trials. In contrast, if CNS considers biomechanical factors during movement, then the response to a cursor jump should reflect the weighting associated with the new target force (Fig. 1D). Subjects performed 10 trials with each cursor jump possibility for each of eight target locations (Fig. 2C, red circles), yielding a total of 400 trials (10 trials * 5 jump/unperturbed options * 8 locations).

Data analysis

We computed the mean value of force produced by each arm during the 200–400-ms time period after the target was reached and then projected the computed force amplitude along the corresponding target direction. An elliptical fit was performed on the computed forces for all targets and for each arm of all participants. The elliptical fit was performed by direct least square fitting (Fitzgibbon et al. 1999). A measure of the directionality of the fit was obtained from the ratio of the ellipse axes. A measure of the dominant direction of force production of each arm was obtained from the angle formed by the main axis of the ellipse and the x-axis of the horizontal plane. The surface of the fitted ellipse was used as a measure of the global contribution of each arm for each configuration, wherein the force produced by each arm was averaged across all target directions.

Experiment 1

To detect significant changes in the preferential direction of force production, we conducted a repeated-measures analysis of variance (rmANOVA) with main-axis orientation as the dependent variable, joint configuration and arm as within-subject independent variables, and handedness as a between-subjects independent variable. To detect significant axis orientation differences across configurations, we conducted a rmANOVA with axis ratio as the dependent variable and arm and joint configuration as within-subject variables, and handedness as a between-subjects variable. To compare the relative contributions of each arm during task performance, we conducted a rmANOVA with the total contribution of each arm as a dependent variable, arm- and joint-configuration as within-subject factors, and handedness as a between-subjects factor. For all tests, sphericity was verified with Mauchly’s test.

Experiment 2

We computed the average force produced by the left arm and the right arm across all unperturbed trials. These average forces were used as baseline measures for the corresponding left and right arm forces. The forces measured during the cursor-jump perturbed trials were compared to these baseline forces to reveal course-corrective force changes induced by each perturbation. For each trial, we computed the difference between the force produced by the right arm and the left arm from 10ms prior to cursor jump to 500ms after the cursor jump.

To test whether the forces produced at target reach differed in relation to cursor jump amplitude, we conducted a rmANOVA with the forces produced by the two arms at target reach as the dependent variable and with body-side and cursor jump amplitude as within-group independent variables for each target. Sphericity was verified with Mauchly's test. To determine the instant at which the corrective force adjustments started to differ across cursor jump amplitudes, we conducted a rmANOVA with the derivative of the force difference as the dependent variable and cursor jump amplitude as the within group variable on every 10-ms window after the cursor jump. To determine whether the force distribution across arms during rapid online corrections is optimized based on biomechanics we extrapolated predictions of the force each arm would produce along the direction of the target force after cursor jump (see Fig. 1D) for each jump amplitude and target from the elliptical fits of the forces obtained during unperturbed trials. Correlational analysis was performed between the predicted and measured forces of the perturbed trials.

Mathematical modeling

Biomechanical and physiological model

We used a two-segment upper-limb model as described in detail previously (Li and Todorov 2007). In this model, each limb is actuated by six muscle groups representing mono-articular flexors (m_1 and m_3) and extensors (m_2 and m_4) at the shoulder and elbow joints, respectively, plus a bi-articular flexor (m_5) and extensor (m_6) spanning both joints (see Fig. 1B). Limb configuration was defined by the two joint angles θ_1 (ventral shoulder flexion) and θ_2 (elbow flexion), with the joint coordinates being mirrored across the two limbs (Fig. 1B). The mechanical model was coupled with a linear, first-order model of muscle tension as a function of neural command. Both arms were modeled identically.

The relationship between end-point force F and joint torque τ is given by:

$$\boldsymbol{\tau} = \mathrm{J}(\theta)^{\mathrm{T}}\mathbf{F}, \tag{2}$$

where $\mathrm{J}(\theta)$ is the Jacobian of the system.

$$\mathrm{J}(\theta) = \begin{bmatrix} -\mathrm{L}_1 \sin(\theta_1) - \mathrm{L}_2 \sin(\theta_1 + \theta_2) & -\mathrm{L}_2 \sin(\theta_1 + \theta_2) \\ \mathrm{L}_1 \cos(\theta_1) + \mathrm{L}_2 \sin(\theta_1 + \theta_2) & \mathrm{L}_2 \cos(\theta_1 + \theta_2) \end{bmatrix} \tag{3}$$

The joint torques are produced by the contraction of the various muscle groups actuating the limb. The torque produced by the contraction of a given muscle group depends on the moment arm (i.e., the distance between the joint's center of rotation and the line of action of the muscle group):

$$\boldsymbol{\tau} = \mathrm{M}(\theta)\mathbf{T} \tag{4}$$

In eq. (4) $\mathbf{T} = [\mathrm{T}_1\ \mathrm{T}_2 \ldots \mathrm{T}_6]^{\mathrm{T}}$ represents muscle group contraction force and $\mathrm{M}(\theta)$ is the moment arm (with $\mathrm{M}_1 = \begin{bmatrix} 4.5 & -2 & 0 & 0 & 4.5 & -2.5 \\ 0 & 0 & 3.2 & -4.5 & 2.3 & -4 \end{bmatrix}$, $\mathrm{M}_2 = \begin{bmatrix} 4.2 & -2 & 0 & 0 & 4.2 & -2.5 \\ 0 & 0 & 3.1 & -4.5 & 2.1 & -4 \end{bmatrix}$ and $\mathrm{M}_3 = \begin{bmatrix} 3.3 & -2 & 0 & 0 & 3.3 & -2.5 \\ 0 & 0 & 3.15 & -4.5 & 2.2 & -4 \end{bmatrix}$ for configuration 1,2 and 3 respectively, see Li and Todorov, 2007 for detailed definition of the values of M). Any change in joint configuration (θ) modifies the Jacobian and the moment arm, impacting, in turn, the relationship between muscle contraction and end-point force.

The tension of each muscle group depends upon its corresponding activation level, length, and velocity (Brown et al. 1999). Because we considered the behavioral task to be isometric and because we focused on forces produced at target reach we neglected changes in muscle length arising from muscle contraction and the effect of contraction velocity. We modeled muscle tension as a second-order, low-pass response to the control input u for the sake of simplicity:

$$\mathrm{t}_{\mathrm{musc}}\dot{\mathrm{T}}_{\mathrm{i}} = \mathrm{k}_{\mathrm{i}} \cdot \mathrm{a}_{\mathrm{i}} - \mathrm{T}_{\mathrm{i}} \tag{5}$$
$$\mathrm{t}_{\mathrm{act}}\dot{\mathrm{a}}_{\mathrm{i}} = \mathrm{u}_{\mathrm{i}} - \mathrm{a}_{\mathrm{i}} \tag{6}$$

In the above equations, the index i corresponds to the number of the different muscle groups (Fig. 1D), such that T_{i} is the tension of the corresponding group i, a_{i} is the activation level, u_{i} is the control input, $\mathrm{t}_{\mathrm{musc}}$ is the muscle group activation time (set to 90 ms) and $\mathrm{t}_{\mathrm{act}}$ (set to 50 ms as in Li and Todorov 2007) is the activation dynamics time. Changing activation dynamics (t_{act} and t_{musc}) had no impact on the results. Although these two parameters influenced the force rise time in accordance with the control input change, they did not affect the steady-state forces reached. k_i is the activation gain of the corresponding muscle group i (k_1=0.87, k_2=0.67, k_3=1.06, k_4=0.58, k_5=0.24, k_6=0.48) and represents the relative strengths of the corresponding muscle group, with a greater activation gain leading to a greater contraction force for a given neural input. The activation gains were estimated from measurements of cross-sectional areas of human cadaver muscles (Crevecoeur and Scott 2014). It is worth noting that activation gains were greater for the flexor muscles for the elbow and shoulder muscle pairs ($k_1 > k_2$ and $k_3 > k_4$) but not for the bi-articular muscle pair ($k_5 < k_6$).

All simulations were based on arms of identical dimensions and strength positioned symmetrically relative to the body midline (Fig. 1B). Indeed, the forces produced in this task are far from maximum voluntary contraction forces. Variability was also considered identical across arms in simulations. To verify this hypothesis we computed the 95% confidence ellipse of the forces produced by each arm across trials and performed a rmANOVA with this measure. This rmANOVA revealed no significant main effect of body-side (F(1,18)=2.89, p=0.1), handedness (F(1,18)=0.08, p=0.78) or target (F(15,270)=1.67, p=0.2) and no significant interaction effect (p>0.16). Joint angles (θ) were the only parameters modified across simulations, which impacted the Jacobian matrix ($J(\theta)$ in Eq. 3) and the moment arms ($M(\theta)$ in Eq. 4, Li and Todorov 2007). Therefore, the biomechanical factors influencing the predicted force distribution across arms are the asymmetries in strength across flexors and extensors muscle groups in each arm, the relation between joint torques and end-point force ($J(\theta)$) and the moment arm of each muscle group ($M(\theta)$ both of which vary with joint configuration).

Optimal Control problem

Because the task requires holding the cursor at the target for 1 s, which involves continuous feedback monitoring to compensate for motor noise, the nominally isometric task becomes effectively a dynamic task. Hence, the question of whether a static solution of a global minimization problem can characterize dynamic control faithfully is nontrivial. Thus, we considered a dynamic control model for the sake of generality.

We employ an optimal feedback control model with a positivity constraint on the neural input, $\mathbf{u} = [\mathrm{u}_1\ \mathrm{u}_2 \dots \mathrm{u}_{12}]^{\mathrm{T}} > 0$. The positivity constraint is necessary to avoid negative control input (and tension) for any muscle group and was applied to represent the physiological property of muscle force generation being limited to contraction (muscles can only pull on the bones). The state-space representation of the system dynamics in discrete time is defined as

$$\mathbf{x}_{\mathbf{t+1}} = \mathrm{A}\mathbf{x}_{\mathbf{t}} + \mathrm{B}\mathbf{u}_{\mathbf{t}} + \boldsymbol{\omega}_{\mathbf{t}} \tag{7}$$

where $\mathbf{x}_{\mathbf{t}} = [\mathbf{x}\ \mathbf{y}\ \mathbf{F}_{\mathbf{x}}^{\mathbf{R}}\ \mathbf{F}_{\mathbf{x}}^{\mathbf{L}}\ \mathbf{F}_{\mathbf{y}}^{\mathbf{R}}\ \mathbf{F}_{\mathbf{y}}^{\mathbf{L}}\ \mathbf{T}_{\mathbf{1}}^{\mathbf{L}} \dots \mathbf{T}_{\mathbf{6}}^{\mathbf{L}}\ \mathbf{T}_{\mathbf{1}}^{\mathbf{R}} \dots \mathbf{T}_{\mathbf{6}}^{\mathbf{R}}\ \mathbf{a}_{\mathbf{1}}^{\mathbf{L}} \dots \mathbf{a}_{\mathbf{6}}^{\mathbf{L}}\ \mathbf{a}_{\mathbf{1}}^{\mathbf{R}} \dots \mathbf{a}_{\mathbf{6}}^{\mathbf{R}}\ \mathbf{x}^{*}\ \mathbf{y}^{*}]$ represents the state of the system at time step *t* and contains endpoint force, muscle tension, and muscle activation values respectively. The variable $\boldsymbol{u}_{\boldsymbol{t}}$ represents the neural input at time t, with $\boldsymbol{\omega}_{\mathbf{t}} \sim \mathrm{N}(0, \Omega_{\omega})$ defining the random Gaussian noise. The covariance of the state noise $\Omega_{\omega}(19{:}30{,}19{:}30) = \mathrm{I}_{12\mathrm{x}12}$ with I being the identity matrix and $\Omega_{\omega}(\mathrm{i}, \mathrm{j}) = 0$ otherwise. With the noise covariance matrix defined in this way, random noise is applied only to the control command. The matrices A and B are defined using the equations detailed above. For simplicity, this model does not include signal-dependent noise, thereby exploiting the separation principle and enabling easy computation of the optimal control and estimation in a closed loop, as is needed to handle the positivity constraint on the muscles. Nevertheless, all aspects of the simulations are expected to generalize with the presence of signal-dependent noise.

The available information about the state of the system is given by:

$$\mathbf{y}_{\mathbf{t}} = \mathrm{C}\mathbf{x}_{\mathbf{t}} + \boldsymbol{\eta}_{\mathbf{t}} \tag{8}$$

where $\boldsymbol{y}$ represents the output of the system, $\mathbf{C} = \mathbf{I_{30}}$ represent the feedback matrix and $\boldsymbol{\eta} \sim \mathrm{N}(0, \Omega_\eta)$ defines the random Gaussian noise applied to the feedback. The covariance of the feedback noise is $\Omega_\eta = \begin{bmatrix} 10^{-3}\mathrm{I}_{30} & \mathrm{O}_{30\mathrm{x}2} \\ \mathrm{O}_{2\mathrm{x}30} & 10^{-10}\mathrm{I}_2 \end{bmatrix}$.

Following computation of the optimal input, we used Kalman filtering to get an unbiased estimate of the state vector that minimizes estimation variance as shown in Eq. (9)

$$\hat{\mathbf{x}}_{\mathbf{t+1}} = \mathrm{A}\hat{\mathbf{x}}_{\mathbf{t}} + \mathrm{B}\mathbf{u}_{\mathbf{t}} + \mathrm{K}_\mathrm{t}(\mathbf{y}_\mathrm{t} - \mathrm{C}\hat{\mathbf{x}}_{\mathbf{t}}). \tag{9}$$

wherein $\hat{\mathrm{x}}$ represents the estimated state of the system and K_t represents the Kalman filter gain.

To compute the optimal neural input $\mathbf{u}$, we minimized the cost function given by

$$\mathrm{V}_\mathrm{t} = \sum_{\mathrm{i}=0}^{\mathrm{N}} \mathbf{x}\big(\mathrm{t}+\mathrm{i}\big|\hat{\mathrm{x}}(\mathrm{t})\big)^\mathrm{T} \mathrm{Q}\mathbf{x}\big(\mathrm{t}+\mathrm{i}\big|\hat{\mathrm{x}}(\mathrm{t})\big) + \mathbf{u}(\mathrm{t}+\mathrm{i})^\mathrm{T}\mathrm{R}\mathbf{u}(\mathrm{t}+\mathrm{i}) \tag{10}$$

In Eq. (10), matrices Q and R define the state and input costs, respectively. The matrix Q penalizes output error and forces differences across the arms. The matrix R penalizes high neural inputs to prevent excessive muscle activation. In our model $\mathrm{R} = 10^{-7}\mathrm{I}_{12}$. Changing this value did not influence the static end-point forces produced by the two arms in the model, but rather affected the time necessary to reach these end-point forces. The finite horizon N is the predictive horizon that allows us to handle the positivity constraints on the vector $\mathbf{u}$. An analytical solution of the unconstrained problem is generated for each time step. If the analytically computed control input $\mathbf{u}$ violates any constraint ($\mathrm{u}_\mathrm{i} < 0$ for some i), quadratic programming is used to find a numerical solution that does not violate the constraint. The quadratic programming algorithm computes a numerical solution for the time window defined by N. Because the noise that may perturb the system during the time window N is unpredictable, we use a receding horizon policy, take the first element of the computed control vector, and restart the process at the next time step.

Developing the first part of eq. (10) gives the following expression:

$$\mathbf{x}^{\mathrm{T}}\mathrm{Q}\mathbf{x} = \mathrm{w}_1(\mathrm{x}-\mathrm{x}^*)^2 + \mathrm{w}_2(\mathrm{y}-\mathrm{y}^*)^2 + \mathrm{w}_3\left(\mathrm{F}_\mathrm{x}^\mathrm{L} - \mathrm{F}_\mathrm{x}^\mathrm{R}\right)^2 + \mathrm{w}_4\left(\mathrm{F}_\mathrm{y}^\mathrm{L} - \mathrm{F}_\mathrm{y}^\mathrm{R}\right)^2 \tag{11}$$

where x and y represent the coordinates of the cursor location, x^* and y^* represent the target coordinates, and the $\mathrm{F}_\mathrm{x}^\mathrm{L}, \mathrm{F}_\mathrm{y}^\mathrm{L}, \mathrm{F}_\mathrm{x}^\mathrm{R}$ and $\mathrm{F}_\mathrm{y}^\mathrm{R}$ variables represent the x and y forces of the left and right arm, relative to each coordinate axis, respectively. Force differences across the two arms were penalized to account for the fact that participants were instructed to use both arms while carrying out the behavioral task (w_3 and w_4 in eq. (11)). In our model, $\mathrm{w}_1 = \mathrm{w}_2 = 1000$ and $\mathrm{w}_3 = \mathrm{w}_4 = 10^{-3}$. The large difference between w_1 and w_2 versus w_3 and w_4 can be explained, in large part, by the factor b (=0.05), which is introduced between the forces produced by the two arms and the cursor position. These parameters were adjusted to limit inter-limb force differences while allowing us to still observe asymmetries in static forces produced by each limb.

The expression of muscle tension in the model was simplified and modeled as a second-order, low-pass response to the control input u, making the system linear. The input u had to be constrained to prevent negative muscle tension in the model. This positivity constraint required using the model predictive control (MPC; Camacho and Bordons, 2007; Rawlings and Mayne, 2012) framework because standard stochastic optimal control models (LQG see Astrom (1970) for details) do not deal directly with bounded solution spaces. However, MPC is similar to the standard model type in principle, with the only difference being that MPC uses quadratic programming to derive a numerical solution to the control problem that meets a positivity constraint.

Results

Optimal weighting of the left and right arms in isometric force production

In Experiment 1, participants were free to modulate the amount of force produced by each arm while generating a total force of 20 N. Model simulations performed using the average joint angles presented in Table 1 predicted that the force produced by each arm would vary depending upon the direction of the target force in a manner that exploits this redundancy (Fig. 2B). Each arm was predicted to have a preferential direction in which it would produce a larger force (Fig. 2B), and this direction changed with joint configuration. In the simulations, control was distributed across the two arms based on their respective preferential directions. Therefore, changing joint configuration in the model impacted the force distribution across the limbs in the simulations. For instance, the left arm produced larger forces in the up-right direction in configuration 1, but produced larger forces in the up-left and down-right directions in configuration 3. In the model, three factors explain these differences in preferential direction of force production across configurations. Firstly, the Jacobian of the system and the moment arm of each muscle group which are both dependent on the joint configuration are the two factors having the greatest impact on the preferential direction of force production. Secondly, differences in strength across the various muscle groups, with flexor muscles being stronger than extensor muscles, also impact the force distribution across arms. The two extreme configurations, 1 and 3 on Fig. 2, were selected because the preferential directions of the two arms were inverted between these two configurations. Configuration 2 was chosen as an intermediate configuration.

The experimental data from right- and left-handed participants followed the same pattern as the model simulations (Fig. 2C and D). The preferential direction of each arm changed progressively across configurations in a way that is similar to the changes observed in model simulations. The preferential direction of the two arms determined the force distribution across limbs. More precisely, the main-axis orientation of the model simulations are good predictions of the main-axis orientation observed in the experimental data for configurations 1 and 3, but not for configuration 2 (Fig. 2B, C and D). A rmANOVA revealed no main effect ($p > 0.2$ in all cases) of handedness ($F(1,18) = 1.425$), body-side (left vs. right arm, $F(1,18) = 3.202$), or joint configuration ($F(2,36) = 1.42$) on the preferential direction of force production. There was a significant interaction between joint-configuration and body-side ($F(2,36) = 40.79$, $p < 0.001$), but no other significant interactions ($p > 0.1$), indicating that joint configuration affected the main-axis orientation differently across the subjects' two arms. More precisely, the influence of joint configuration on the main-axis orientation of the left arm was the inverse of its influence on the main-axis orientation of the right arm (Fig. 2B–D and Fig. 3D). Bonferroni post hoc tests revealed that main-axis orientation differed significantly across joint configurations for both arms ($p < 0.05$ in all cases). Moreover, the main-axis orientations of the left and right arm differed significantly from each other in configurations 1 and 3 ($p < 0.001$ in both cases) but not in configuration 2.

To understand how the preferential direction of force production of the two arms transitions between configuration 1 and configuration 3, we varied the simulated elbow angles of the model continuously from 35° to 110°, we also varied the shoulder angles linearly across the values measured for configurations 1, 2 and 3 (see Table 1). We measured the preferential direction of force production and the overall contribution of each arm using an elliptical fit (see methods). The directional preference of each arm was measured as the orientation of the main axis of the fitted ellipses. Data from the simulations (Fig. 3A) and from an exemplar participant (Fig. 3B) in configuration 1 are shown in Fig. 3, note the elliptical fit performed as well as the main axis of the ellipse. Simulations across elbow angles showed a progressive transition of the preferential direction of force production of the two arms relative to the elbow angle (Fig. 3C). In simulations, the preferential directions of the two arms reversed at the same elbow angle of 86°. More precisely, when the elbow angle reached 86°, the preferential direction of the left arm changed from lying in the down-left to up-right direction towards lying in the up-left to down-right direction and vice versa for the right arm. Experimental results of all participants pooled together showed similar behavior except that the transition angle was ~76°, corresponding to a smaller elbow angle close to configuration 2 (Fig. 3D). The gradual transition observed in the simulations (Fig. 3C) is also observed in our experimental observations (Fig. 3D), however a general shift towards larger elbow angles is observed in simulations when compared to experimental data. It is possible that no significant difference in preferential direction was observed in configuration 2 in our experiment because the elbow angle in configuration 2 (76.51 ± 5.70°) is closer to the reversal point of experimental results than the elbow angle of configuration 1 (88.53 ± 5.08).

The axis ratio of the fitted ellipse showed a maximum at the switching point in both the simulation and experimental results (Fig. 3E and F). At the switching point, the elliptical fits were almost circular, rendering the extraction of the main axis orientation very sensitive to variability in the data. A rmANOVA revealed a significant main effect of joint configuration (F(2,36) = 4.535, p = 0.0175), but not of body-side (F(1,18) = 2.02, p = 0.173) or handedness (F(1,18) = 0.519, p = 0.48), on axis ratio and no significant interactions (p > 0.1). A post hoc analysis with adjusted paired t-tests (Fig. 3F) revealed that the axis ratio of configuration 2 differed significantly from that of configuration 1 for both arms (p < 0.001), as well as from that of configuration 3 for the right arm (p = 0.027), but not the left arm (p = 0.09). The axis ratio did not differ between configurations 1 and 3 for either arm.

Altogether the model qualitatively predicted the transitions in main axis orientation across configurations (Fig. 3 C-D), as well as the increase followed by a decrease in the axis ratio (Fig. 3 E-F). The model quantitatively predicted main axis orientation of configurations 1 and 3 (Fig. 4, A-C).

The measured main-axis orientations in configurations 1 ($136.6 \pm 21.1°$ for the right arm and $53.15 \pm 13.96°$ for the left arm) and 3 ($66.85 \pm 39.54°$ for the right arm and $123.08 \pm 29.2°$ for the left arm) were, on average, close to the axis orientations predicted by our model simulations (123.7° and 56.2° for the right and left arm in configuration 1 and 44.52° and 135.8° for the right and left arm in configuration 3, Fig. 4A and C). In configuration 2, the measured main-axis orientations ($94.42 \pm 53.24°$ for the right arm and $83.41 \pm 37.87°$ for the left arm) were found to be highly variable due to the proximity of this configuration to the elbow angle of reversal (Fig. 3C). In addition, the near-circularity of the elliptical fits reduced the reliability of our ellipse orientation estimates (Configuration 2, Fig. 4B). The elliptical fits for configurations 1 and 3 had smaller axis ratios than those of configuration 2, enabling less variable main axis estimates. No differences emerged between left- and right-handed participants in any of the three configurations. In terms of main axis orientation the model explained 29% of the variability of the data across the three configurations and 63% when considering only the two extreme configurations (1 and 3).

Finally, while simulations predicted the progressive change of main-axis orientations across configurations, differences can be observed between simulations and experimental data. As in the model the two arms are modeled identically, the force produced by the two arms in simulations are symmetrical relative to the vertical midline whereas asymmetries can be observed between the right and left arm in experimental data (Fig. 2). This suggests that factors other than biomechanics influence participants' behavior. Differences between model simulations and experimental data are not systematic across experimental groups, however similar asymmetries can be observed in both right- and left-handed participants. For instance, we determined the total amount of force generated by each arm based on the surface areas of the fitted ellipses for each arm of each subject. We found that the left arm produced, on average, slightly more force (56% and 53% of the total force for left-handed and right-handed participants, respectively) than the right arm (44% and 47%, respectively). A rmANOVA revealed no main effects of handedness ($F(1,18) = 0.207$, $p = 0.61$), body-side ($F(1,18) = 4.18$, $p = 0.056$), or joint configuration ($F(2,36) = 0.613$, $p = 0.55$) on fitted ellipse surface area, and no significant interactions (all $p > 0.2$). The fact that both right- and left-handed groups showed similar asymmetries across arms suggests that these differences are not due to handedness.

Effect of biomechanics on corrective bimanual responses

In Experiment 2, the cursor jumped perpendicularly to the target direction at the midpoint of the movement requiring participants to perform corrective force adjustments to direct the cursor towards the target. These corrective force adjustments produced in response to cursor jumps differed dependent on the direction of the target (Fig. 5C, D, G and H). For example, the motor response of the right arm was larger when moving the cursor towards the lower target than towards the higher target (Fig. 5G and C, inset respectively). The end-point forces produced during unperturbed trials were similar to Experiment 1 in configuration 3, thus reproducing the Experiment 1 results in a distinct group of participants (see Fig. 6A and Fig. 2C-D). As predicted by the model simulation, the main differences in force produced by the two arms in configuration 3 were seen for the down-right and down-left targets. If motor corrections take biomechanical factors into account, then lateral jumps should evoke online adjustments of the weighing of each arm on the total force production that differ according to the location of the target and to the amplitude of the cursor-jump. For instance, perturbations when moving the cursor towards a straight downward target should elicit distinct corrections dependent on the direction of the cursor jump, with a greater contribution of the right or left arm when the cursor jumps clockwise (CW) or counter clockwise (CCW) respectively (Fig. 6A, B and C).

Analysis of the average end-point forces produced in perturbed trials towards the center-down target revealed adjustments consistent with the biomechanically optimal distribution of forces (Fig. 6A and B). More precisely, for the center-down target, motor corrections to CCW or CW jumps elicited differential use of the arms that paralleled the differences observed at baseline (Fig. 6B).

A series of rmANOVAs was performed for each target on the forces produced by each arm. For the up-right and up-left (diagonal direction) targets, as well as the far-right and far-left targets (along the x-axis), there was a main effect of perturbation (individual tests across target $F(4,48) > 7$, $p < 0.05$), no effect of body-side ($F(1,12) < 1.8$, $p > 0.05$), and no interaction ($F(4,48) < 2.3$, $p > 0.1$). A significant effect of perturbation shows that for these targets the cursor jump amplitude and direction impacts the end-point forces produced by the two arms. For the down-left and down target, we found a main effect of perturbation ($F(4,48) = 36.5$, $p < 0.001$ and $F(4,48) = 7.4$, $p < 0.001$ respectively), no effect of body-side ($F(1,12) = 1.8$, $p = 0.184$ and $F(1,12) = 7.4$, $p = 0.077$ respectively), and a significant interaction ($F(4,48) = 9.8$, $p < 0.001$ and $F(4,48) = 49.6$, $p < 0.001$ respectively). For the down-right target, we found main effects of perturbation ($F(4,48) = 12.6$, $p < 0.001$), body-side ($F(1,12) = 7.5$, $p = 0.017$) and a significant interaction ($F(4,48) = 1.8$, $p = 0.133$). More intuitively, a significant interaction effect means that force adjustments of the dominant arm changed across cursor jump amplitudes in a different way than the force adjustments of the non-dominant arm (Fig. 6B).

For each perturbation amplitude, we computed the difference between the forces produced by the right and left arms from 200 ms before to 500 ms after the cursor jump. For all targets, corrective responses started, on average, 160 ms after the cursor jump (Fig. 6C), though the adjustments differed with respect to the target direction (reported above). After 160 ms the weight attributed to each arm on the total force production is modulated online dependent on the cursor jump amplitude (Fig. 6C). To determine the moment at which the inter-arm force difference started to diverge across jump amplitudes, we computed the derivative of the force difference between the right and left arms. With this derivative as the dependent variable, we performed a rmANOVA on each 10-ms window starting from the moment of the jump. For the center-down target, we observed a main effect of jump amplitude ($F(4,48) = 3.617$, $p < 0.05$) starting from ~160 ms after the jump (all earlier windows, $p > 0.05$). This correction latency was later than expected in light of previous reports on online corrections during reaching (Dimitriou et al. 2013). Notwithstanding, similar correction times (~150 ms) were observed with a unimanual version of the task (data not shown). It is worth noting that while the net response of the arms scales with direction and amplitude of the cursor jump, the force difference across arms is precisely indicative of the influence of biomechanics in the corrective response, with adjustments differing dependent on target direction in a way that is consistent with the force distribution predicted by joint configuration (Fig. 6A). For instance, for the upper target no change in force difference across arms should arise from a left or right-ward cursor jump (Fig. 6A), which is what we observed in the time evolution of the perturbed trials towards this target (data not shown).

The force distribution across arms observed after cursor jumps was very similar to the force distribution observed during unperturbed trials for the corresponding direction (Fig. 7A and D) suggesting that biomechanics impacted the corrective force responses. To further compare the end-point forces of unperturbed and perturbed trials, we fitted an ellipse on the end-point forces measured during unperturbed trials. Based on this elliptical fit we predicted the forces that should be produced in the direction of the new target forces after cursor jump. We compared the predicted force difference between right and left arm to the forces measured during perturbed trials and observed that the correlations between predicted and measured forces for each cursor jump amplitude were very strong ($R^2 > 0.80$ and $p < 0.001$; Fig. 7B, C, E and F), confirming that biomechanical factors were integrated into online corrective force adjustments. We performed the same analysis with model simulations and observed correlations very similar to those observed in experimental data (Fig 7B, C, E, F).

Discussion

We investigated the impact of biomechanical constraints on how the brain weights each arm in the context of bimanual control. More precisely, we studied the impact of asymmetries in the strength across muscle groups of the upper-limbs and the effect of the moment arm of each limb joint and of each muscle group which varied with joint configuration. Our main finding was that the orientation of the axes at which each limb produces more force (ellipse orientation) and how much force production varies across the targets (axis ratio) varied progressively and systematically across joint configurations, independent of handedness, in a way that was predicted by simulations of the optimal control model, in which differences in force across flexor and extensor muscle groups and the moment arm of each upper-limb joint as well as of each muscle group were the only source of mechanical anisotropy. Moreover, following cursor jumps the forces produced by participants were adjusted online optimally with respect to the biomechanical configuration of their arms. The presently observed match between the optimal control model and participants' behavior supports the hypothesis that biomechanics shape neural control solutions during bimanual tasks.

With respect to laterality, there are several known asymmetries between the dominant and non-dominant arm during unimanual movements (see Goble and Brown, 2008 for review). For instance, Sainburg and Kalakanis (2000) reported a laterality difference in the control of limb dynamics during reaching. Shabbott and Sainburg (2008) further explored this difference in response to cursor jumps during unimanual reaching movements and found that the right and left arm showed similar timing and amplitude of corrective movements but showed differences in movement trajectories. Mutha et al. (2013) suggested that, when learning to reach in a force field, the dominant hand is better at optimizing task dynamics whereas the non-dominant hand is better at stabilizing around the target.

Handedness has also been shown to influence bimanual coordination. Control of the dominant arm, relative to the non-dominant arm, has been associated with a smaller variability (Kalisch et al. 2006), and thus better motor control, for which variability and effort are determinant factors (Todorov and Jordan 2002). In a task similar to the one presented here, Salimpour and Shadmehr (2014) reported a smaller variability in force production for the dominant arm, which led to a greater contribution of this arm during bimanual task performance. White and Diedrichsen (2010) reported that the left hand of right-handed participants corrected more following unexpected visuomotor rotations, but also adapted more in the next trial, suggesting that the CNS may assign error-coping to the non-dominant (and less skilled) arm. Altogether, these findings indicate that cerebral lateralization impacts control across a wide range of contexts.

Surprisingly, our experimental observations from right-handed and left-handed participants in Experiment 1 were identical in terms of overall contribution and preferential direction of force production. Furthermore, in Experiment 2, we found no effect of handedness on the corrective responses for any of the participants, thus we were not able to analyze how lateralization may interact with the optimization related to limb biomechanics. Given that two prior studies that employed the same paradigm found influences of handedness on the inter-arm distribution of force (Salimpour and Shadmehr 2014; Salimpour et al. 2015), our data suggests that the circumstances under which handedness may influence bimanual control deserve further examination. As to why we did not find an influence of handedness, it is possible that our explicit instruction to use both arms influenced the way the task was performed. It is also possible that as the rather low level of forces produced during the task lead to small differences in variability across arms, which we did not measure in a unimanual context as in Salimpour and Shadmehr (2014), but the force level being the same as in this study it remains unclear where differences between our and previous observations come from. Constraining the arms' position may also have prevented an influence of handedness suggesting that these factors may be hierarchically considered during bimanual manipulations. Indeed, it is conceivable that, if the physics of the task is not experimentally imposed (by constraining the configuration), then participants may adopt a configuration in which the mechanical anisotropies play a secondary role and exploit hand dominance to a greater extent.

Importantly, we found that rapid adjustments following cursor jumps, which alter target-bound forces, were also influenced by the optimal weighting of each limb as predicted by the model (Fig. 7). That is, the perturbation-compelled force adjustments were generated in a way that integrated optimal limb use. The presently observed motor response to reaching the end-point was delayed by ~160 ms, which, in light of previous work, seems fairly long. Electromyographic responses to cursor jumps have been detected with delays of ~100 ms (Dimitriou et al. 2013; Cluff et al. 2015) and around 120–150 ms after reaching the movement end-point in unimanual reaching tasks (Saunders and Knill 2003, 2004; Franklin and Wolpert 2008; Dimitriou et al. 2013). However, our observation of similar response latencies in a unimanual mode of the task suggests that the mapping of force production to cursor motion in this paradigm may require more internal processing than standard reaching tasks. Functional similarity between motor planning and feedback control appears to be a hallmark of sensorimotor coordination (see Crevecoeur et al., 2014; Scott et al., 2015 for review) in the sense that corrective responses exhibit flexibility similar to that of unperturbed movements. Our data suggest that neural resources that optimize control distribution across limbs may be shared between movement planning and movement execution during bimanual tasks.

In our task, three biomechanical parameters influence the force distribution across arms, the relation between joint torques and end-point force ($\mathrm{J}(\theta)$ in the model), the moment arm of each muscle group ($\mathrm{M}(\theta)$) and the asymmetries in force between the flexor and extensors muscle groups.

Previous studies have shown that biomechanical parameters such as the inertial resistance of the arm (Gordon et al. 1994) or the metabolic energy required for movement production (Shadmehr et al. 2016) define preferential direction of reaching movements. Factors such as the inertial resistance of the arm have no impact during isometric tasks as no movement is involved which suggests that some biomechanical factors underlying preferential directions of movement or force production are specific to the type of task being performed. However, despite different biomechanical factors influencing isometric and dynamical tasks, it has been shown that neurons in the primary motor cortex fire preferentially for elbow flexion combined with shoulder extension or elbow extension combined with shoulder flexion, arrangements that are optimized for limb biomechanics in both isometric and dynamical tasks (Scott et al. 2001; Lillicrap and Scott 2013; Heming et al. 2016). Intuitively, the preferential directions that we observed in configurations 1 and 3 correspond with this behavior. Indeed, for each configuration, the directions of largest force production of each arm in our simulations corresponded to these combined flexor-extensor arrangements (data not shown). Hence, the distribution of preferential firing directions of motor cortex neurons, shaped by limb physics, may be an easy and effective way to optimize control solutions during both isometric and dynamical tasks, in a way that may be relatively independent of handedness. An important challenge for future work will be to investigate the neural basis of optimal sharing of effort across limbs in more detail.

In conclusion, we demonstrated a consistent influence of limb physics on the planning and control of bimanual tasks by imposing the direction of force targets. Given the influence of expected motor costs on decisions about how to move (Cisek 2012; Wolpert and Landy 2012), or which target to acquire, our results may also explain possible planning biases during bimanual control. Insofar as a representation of mechanical effort is available during motor planning, we would expect it to impact solution selection. Indeed, for bimanual motor behaviors, our brain may choose a favorable joint configuration as well as a movement plan that is favorable to our limb physics. If so, movement control in general, from planning through execution, may factor in both movement value and biomechanical costs. We expect that prospective studies investigate these question in detail.

Grants

This work was supported by a grant from ESA (European Space Agency), Prodex (BELSPO, Belgian Federal Government), IAP VII 19 DYSCO (BELSPO, Belgian Federal Government).

Disclosures

No conflicts of interest, financial or otherwise, are declared by the authors.

References

Astrom KJ. Introduction to Stochastic Control Theory. Elsevier.

Brown IE, **Cheng EJ**, **Loeb GE**. Measured and modeled properties of mammalian skeletal muscle. II. The effects of stimulus frequency on force-length and force-velocity relationships. *J Muscle Res Cell Motil* 20: 627–643, 1999.

Camacho EF, **Bordons C**. Model Predictive control. Springer London.

Cisek P. Making decisions through a distributed consensus. *Curr Opin Neurobiol* 22: 927–36, 2012.

Cluff T, **Crevecoeur F**, **Scott SH**. A perspective on multisensory integration and rapid perturbation responses. *Vision Res* 110: 215–222, 2015.

Cos I, **Belanger N**, **Cisek P**. The influence of predicted arm biomechanics on decision making. *J Neurophysiol* 105: 3022–3033, 2011.

Cos I, **Girard B**, **Cisek P**. A Modelling Perspective on the Role of Biomechanics on Motor Decision-Making [Online]. *NeuroComp / KEOpS'12 Work.* http://www.isir.upmc.fr/files/2012ACTN2714.pdf.

Cos I, **Khamassi M**, **Girard B**. Modelling the learning of biomechanics and visual planning for decision-making of motor actions. *J Physiol* 107: 399–408, 2013.

Crevecoeur F, **Cluff T**, **Scott SH**. Computational approaches for goal-directed movement planning and execution. In: *The Cognitive Neurosciences*, edited by MS G, GR M. MIT Press, p. 461–475.

Crevecoeur F, **Scott SH**. Beyond Muscles Stiffness: Importance of State-Estimation to Account for Very Fast Motor Corrections. *PLoS Comput Biol* 10: e1003869, 2014.

Dimitriou M, **Wolpert DM**, **Franklin DW**. The Temporal Evolution of Feedback Gains Rapidly Update to Task Demands. *J Neurosci* 33: 10898–10909, 2013.

Dounskaia N, **Goble JA**, **Wang W**. The role of intrinsic factors in control of arm movement direction: implications from directional preferences. *J Neurophysiol* 105: 999–1010, 2011.

Dounskaia N, **Wang W**, **Sainburg RL**, **Przybyla A**. Preferred directions of arm movements are independent of visual perception of spatial directions. *Exp Brain Res* 232: 575–586, 2014.

Fitzgibbon A, **Pilu M**, **Fisher R**. Direct least square fitting of ellipses. *IEEE Trans Pattern Anal Mach Intell* 21: 476–480, 1999.

Franklin DW, **Wolpert DM**. Specificity of reflex adaptation for task-relevant variability. *J Neurosci* 28: 14165–14175, 2008.

Goble DJ, **Brown SH**. The biological and behavioral basis of upper limb asymmetries in sensorimotor performance. *Neurosci Biobehav Rev* 32: 598–610, 2008.

Gordon J, **Ghilardi MF**, **Cooper SE**, **Ghez C**. Accuracy of planar reaching movements - II. Systematic extent errors resulting from inertial anisotropy. *Exp Brain Res* 99: 112–130, 1994.

Gribble PL, **Ostry DJ**. Compensation for interaction torques during single- and multijoint limb movement. [Online]. *J Neurophysiol* 82: 2310–26, 1999. http://www.ncbi.nlm.nih.gov/pubmed/10561408.

Heming EA, **Lillicrap TP**, **Omrani M**, **Herter TM**, **Pruszynski JA**, **Scott SH**. Primary motor cortex neurons classified in a postural task predict muscle activation patterns in a reaching task. *J. Neurophysiol.* (2016). doi: 10.1152/jn.00971.2015.

Hollerbach JM, **Flash T**. Dynamic interactions between limb segments during planar arm movement. *Biol Cybern* 44: 67–77, 1982.

Kalisch T, **Wilimzig C**, **Kleibel N**, **Tegenthoff M**, **Dinse HR**. Age-related attenuation of dominant hand superiority. *PLoS One* 1: e90, 2006.

Kawakami Y, **Nakazawa K**, **Fujimoto T**, **Nozaki D**, **Miyashita M**, **Fukunaga T**. Specific tension of elbow flexor and extensor muscles based on magnetic resonance imaging. *Eur J Appl Physiol Occup Physiol* 68: 139–147, 1994.

Li W, **Todorov E**. Iterative linearization methods for approximately optimal control and estimation of non-linear stochastic system. *Int J Control* 80: 1439–1453, 2007.

Lillicrap TP, **Scott SH**. Preference distributions of primary motor cortex neurons reflect control solutions optimized for limb biomechanics. *Neuron* 77: 168–79, 2013.

Mutha PK, **Haaland KY**, **Sainburg RL**. Rethinking motor lateralization: specialized but complementary mechanisms for motor control of each arm. *PLoS One* 8: e58582, 2013.

O'Sullivan I, **Burdet E**, **Diedrichsen J**. Dissociating variability and effort as determinants of coordination. *PLoS Comput Biol* 5: e1000345, 2009.

Oldfield R. The assessment and analysis of handedness: The Edinburgh inventory. *Neuropsychologia* 9: 97–113, 1971.

Rawlings JB, **Mayne DQ**. Model Predictive Control : Theory and Design. .

Sabes PN, **Jordan MI**, **Wolpert DM**. The role of inertial sensitivity in motor planning. [Online]. *J Neurosci* 18: 5948–57, 1998. http://www.ncbi.nlm.nih.gov/pubmed/9671681.

Sainburg RL. Evidence for a dynamic-dominance hypothesis of handedness. *Exp brain Res* 142: 241–58, 2002.

Sainburg RL, **Kalakanis D**. Differences in control of limb dynamics during dominant and nondominant arm reaching. *J Neurophysiol* 83: 2661–2675, 2000.

Salimpour Y, **Mari ZK**, **Shadmehr R**. Altering Effort Costs in Parkinson's Disease with Noninvasive Cortical Stimulation. *J Neurosci* 35: 12287–302, 2015.

Salimpour Y, **Shadmehr R**. Motor costs and the coordination of the two arms. *J Neurosci* 34: 1806–18, 2014.

Saunders JA, **Knill DC**. Humans use continuous visual feedback from the hand to control fast reaching movements. *Exp brain Res* 152: 341–52, 2003.

Saunders JA, **Knill DC**. Visual feedback control of hand movements. *J Neurosci* 24: 3223–34, 2004.

Schweighofer N, **Xiao Y**, **Kim S**, **Yoshioka T**, **Gordon J**, **Osu R**. Effort, success, and nonuse determine arm choice. *J Neurophysiol* 114: 551–559, 2015.

Scott SH, **Cluff T**, **Lowrey CR**, **Takei T**. Feedback control during voluntary motor actions. *Curr Opin Neurobiol* 33: 85–94, 2015.

Scott SH, **Gribble PL**, **Graham KM**, **Cabel DW**. Dissociation between hand motion and population vectors from neural activity in motor cortex. *Nature* 413: 161–165, 2001.

Shabbott B a, **Sainburg RL**. Differentiating between two models of motor lateralization. *J Neurophysiol* 100: 565–575, 2008.

Shadmehr R, **Huang HJ**, **Ahmed AA**. A Representation of Effort in Decision-Making and Motor Control. *Curr Biol* 26: 1929–34, 2016.

Swinnen SP, **Jardin K**, **Meulenbroek R**. Between-limb asynchronies during bimanual coordination: Effects of manual dominance and attentional cueing. *Neuropsychologia* 34: 1203–1213, 1996.

Todorov E, **Jordan MI**. Optimal feedback control as a theory of motor coordination. *Nat Neurosci* 5: 1226–35, 2002.

Wang W, **Johnson T**, **Sainburg RL**, **Dounskaia N**. Interlimb differences of directional biases for stroke production. *Exp Brain Res* 216: 263–274, 2012.

White O, **Diedrichsen J**. Responsibility assignment in redundant systems. *Curr Biol* 20: 1290–5, 2010.

Wolpert DM, **Landy MS**. Motor control is decision-making. *Curr Opin Neurobiol* 22: 996–1003, 2012.

Figure captions

Figure 1. Human-inspired model and experimental procedure performed on the KINARM robot. A) Each subject sat in front of a screen holding two robotic arm handles. Movements were countered by a very stiff force field (k = 2000 N/m, B = 50 N·s/m). Participants are asked to push on both handles to reach a total force of 20 N in the horizontal plane. A cursor (black dot) indicated the total force being produced. The sum of forces produced by both arms was mapped onto the cursor position (black dot) on the virtual reality display. **B)** Two human-inspired upper-limbs actuated by six muscle groups (numbered 1–6) corresponding to the mono- and bi-articular muscles at each joint. Both limbs work in the horizontal plane. The joint configuration was defined by the joint angles θ_1 and θ_2. **C)** The possible targets (black and red circles) were positioned on a 10-cm–radius circle and evenly spaced. Targets represented by black and red circles were used in experiment 1 and only the targets represented by red targets were used in experiment 2. **D)** Cursor trajectory (solid black line) from the initial cursor position to the target center in experiments 1 and 2. The force produced by the subject is presented as a gray line. In experiment 2, the cursor jumped midway through the movement. The target projected onto the screen was presented as a black circle. The new target force after the cursor jump is presented as a dashed gray disk.

Figure 2. Arm configuration, model predictions, and mean experimental results for right- and left-handed participants. A) The three joint configurations tested in model simulations and experiments. **B)** In the simulations, the force produced by each arm was projected along the direction of the target and plotted in the target's direction. Solid grid lines show target directions and force levels. Simulation results are plotted in red for the right arm and in blue for the left arm. The main axis orientation of an elliptical fit performed on simulation data is presented as a solid blue or red line. **C)** Mean and standard error of the mean (SEM) of the experimental results of all right-handed participants pooled together. The forces are displayed in a manner identical to the simulation results. The solid lines represent the mean main-axis orientations of the arms of all right-handed participants pooled together. **D)** Mean and SEM of the experimental results of all left-handed

participants pooled together. The lines represent the pooled mean main-axis orientations as in panel C.

Figure 3. Main-axis orientation and axis ratio for simulations at various elbow angles and for experimental data. A) Simulation data for the left (blue dots) and right arm (red dots) in configuration 1. The elliptical fit performed on these data is presented as a solid line ellipse. The main axis orientation of the fitted ellipses are presented as solid lines. **B)** Exemplar participant data for the left and right arm (blue and right disks, respectively). The elliptical fit is presented as a solid line ellipse. The main axis orientation of the ellipse is presented as a solid line. **C)** Main-axis orientation of the left (blue line) and right arm (red line) of the simulations for elbow angles ranging from 35° to 110°. Shoulder angles were linearly interpolated between the angles presented in Table 1 in order to match the experimental joint configurations as closely as possible. The dashed gray lines indicate the elbow angles measured during the experiment for configurations 1, 2, and 3. **D)** Main-axis orientation for the left (blue line) and right arm (red line) of all participants pooled together for the three tested configurations. **E)** Axis ratio for the two arms in the simulations (black line). Both arms had an identical axis ratio. **F)** Axis ratio for the left and right arm of all participants pooled together for the three configurations.

Figure 4. Radial plot of the axis ratio and main-axis orientation for all right-handed and left-handed participants in the three experimental configurations. The radius of the plot represents the axis ratio and the phase represents the main-axis orientation of the ellipses fitted on participant data. The right- and left-arm data of all participants are presented in red and blue, respectively. The right-handed participants’ data are presented as disks and the left-handed participants’ data are presented as circles. The main-axis orientation of simulation predictions are presented as solid lines.

Figure 5. Cursor trajectory and arm forces for the top (A–D) and bottom (E–H) targets in exemplar subjects. A, E) Theoretical cursor trajectories of the presented trials for the top (A) and bottom (E) targets. **B, F)** Cursor trajectory of 10 trials for the top (B) and bottom (F) targets with a 5-

cm rightward cursor jump. **C, G)** Corrective force responses (dashed box) of the right (red) and left (blue) arms over 10 trials after cursor jumps (black dots). **D, H)** Time evolution of the x and y forces of the arms for 10 top-target (D) and 10 bottom-target (H) trials.

Figure 6. Analysis of corrective responses for all cursor jump amplitudes for the bottom target (positioned at 270°). A) Mean ± SEM of forces produced at target reach for unperturbed trials of all targets. The forces produced by the right (red) and left (blue) arm are projected along the direction of the respective target and plotted in the targets direction. Solid grid lines show the target directions and force levels. Cursor jump directions are indicated by white and gray arrows. The actual endpoint forces that must be produced following a cursor jump are presented as white and gray dashed-circle targets (colors match corresponding jumps). **B)** Mean ± SEM of forces produced from 200ms after target reach to 400ms after target reach by the left and right arm for the bottom target with all cursor jump amplitudes. **C)** Time evolution of the average difference between the force produced by the right versus the left arm for all perturbed and unperturbed trials with bottom targets. Shaded areas represent the SEM across participants. Perturbation amplitudes are color-coded: red, 5 cm; green, 3 cm; black, unperturbed; light blue, -3 cm; and purple, -5 cm.

Figure 7. Comparison between forces produced during baseline trials and perturbed trials (A and D) and comparison between forces predicted from baseline trials versus measured forces in all perturbed (B, C, E andF) trials. A, D) Means ± SEMs of forces produced at target reach in unperturbed (A) and perturbed (D) trials for all targets. The forces produced by the right (red) and left (blue) arm are projected along the direction of the respective target and plotted in the targets direction. Solid grid lines show the different target directions and force levels. The light blue circle, square, and diamond represent the corresponding targets in all panels of the plot. The two arrows indicate CCW and CW corrections. **B, E)** Means ± SEMs of measured versus predicted force differences between the right and the left arms for each target in all perturbed trials with -5 cm (B) or 5 cm (E) cursor jumps, which correspond to a large CW (B) or CCW (E) cursor jumps forces. The

predicted force differences were extracted from the ellipses fitted on the forces measured for each arm of each subject during unperturbed trials. A dashed black line represents the unity line. The solid green line represents the predictions of model simulations. The light blue square, circle, and diamond correspond to the targets presented in panel A. **C, F)** Means ± SEMs of measured versus predicted force differences between the right and the left arms for each target in all perturbed trials with -3 cm (C) or 3 cm (F) cursor jumps, which correspond to a small CW (C) or CCW (F) cursor jumps. The solid green line represents the predictions of model simulations. The light blue square, circle and diamond correspond to the targets presented in panel A. Statistical values are shown to the right of all graphs.

Table 1. Mean joint angles (±standard deviations) for all participants. Values reflect averages of all participants pooled together in the three configurations of experiment 1.

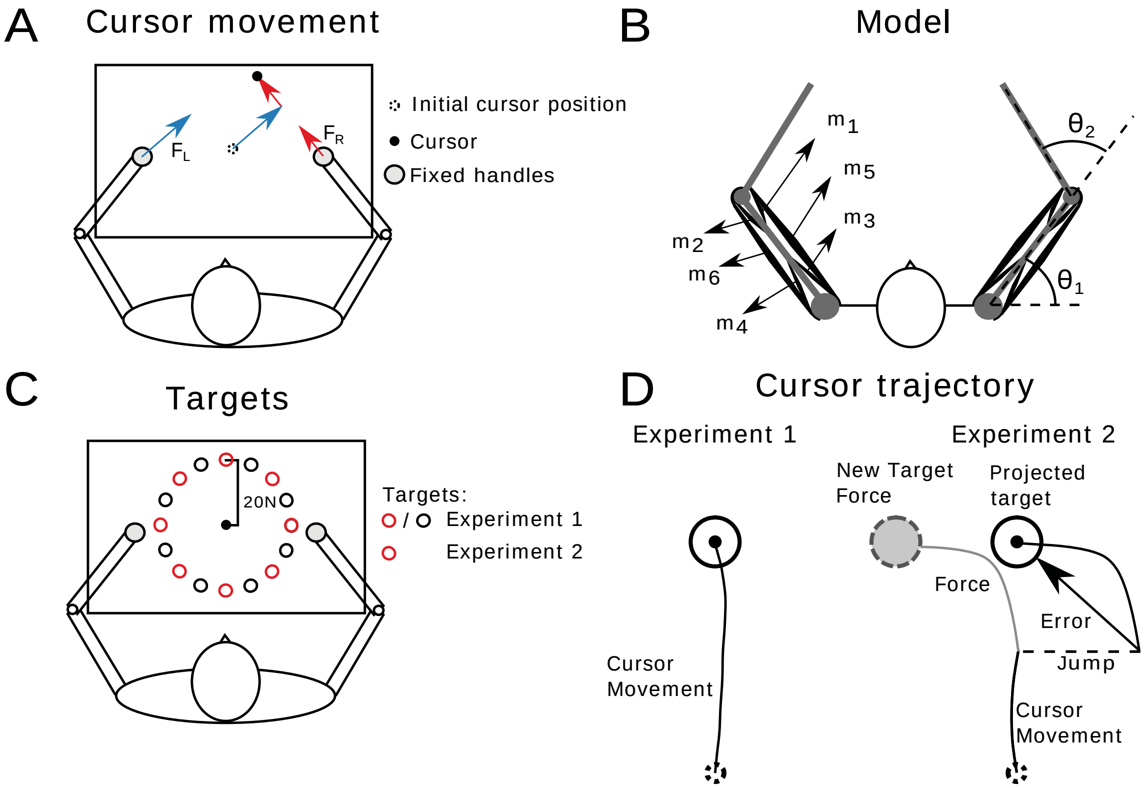
A
Cursor movement
F_L
F_R
Initial cursor position
Cursor
Fixed handles
B
Model
m_1
m_5
m_3
m_2
m_6
m_4
θ_2
θ_1
C
Targets
20N
Targets:
Experiment 1
Experiment 2
D
Cursor trajectory
Experiment 1
Experiment 2
New Target Force
Projected target
Force
Error
Jump
Cursor Movement
Cursor Movement

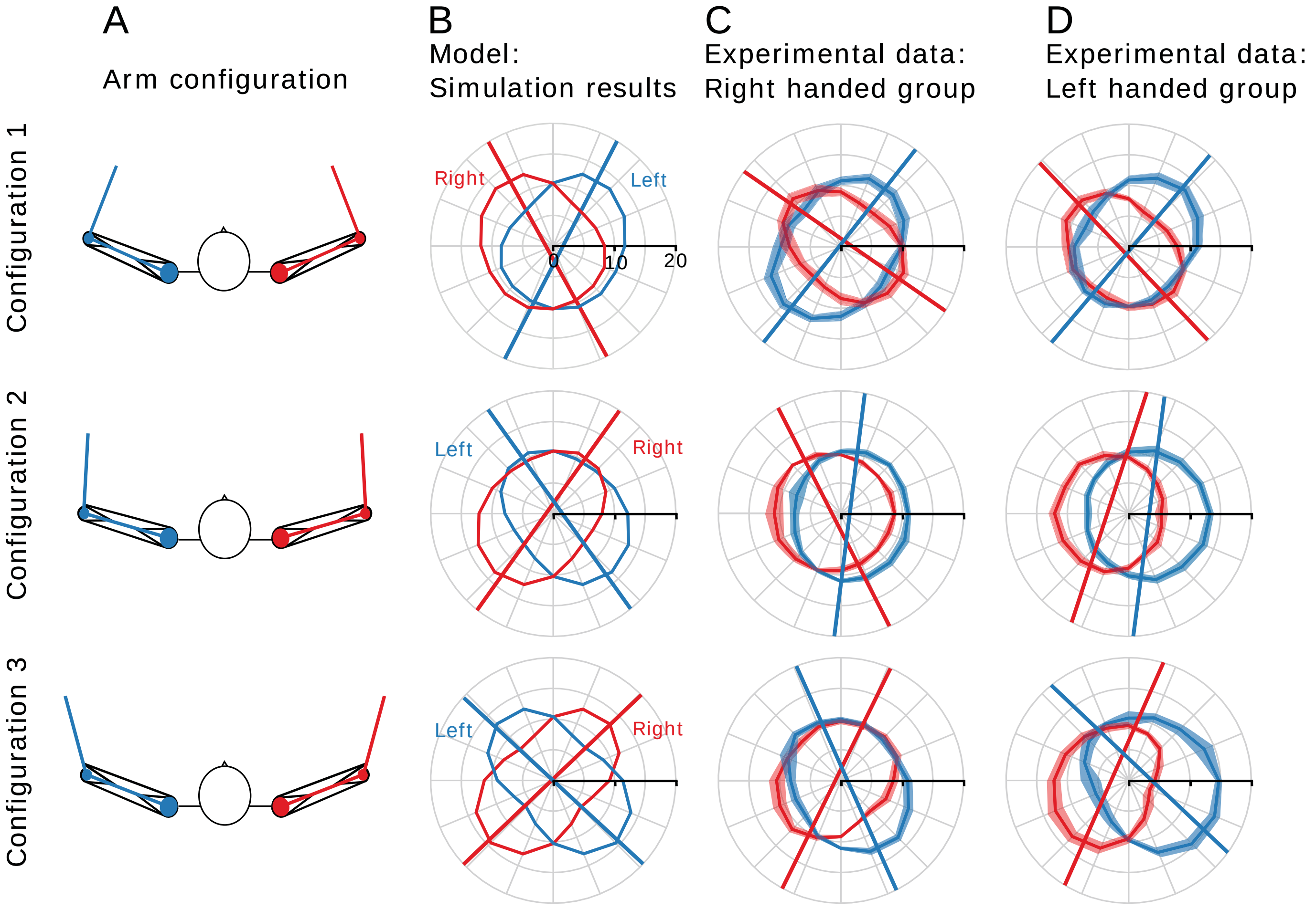
A
Arm configuration
B
Model:
Simulation results
C
Experimental data:
Right handed group
D
Experimental data:
Left handed group
Configuration 1
Configuration 2
Configuration 3
Right
Left
0
10
20
Left
Right
Left
Right

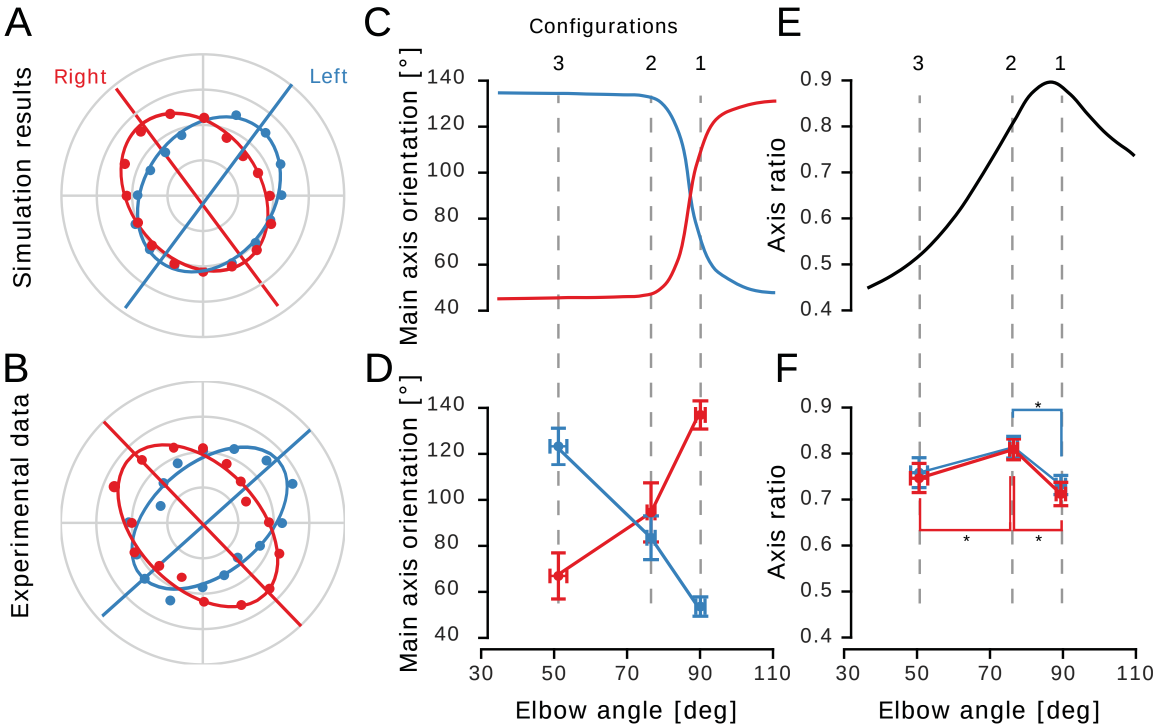A
Simulation results
Right
Left
B
Experimental data
C
Configurations
3
2
1
Main axis orientation [°]
140
120
100
80
60
40
D
E
Axis ratio
0.9
0.8
0.7
0.6
0.5
0.4
F
*
30
50
70
90
110
Elbow angle [deg]

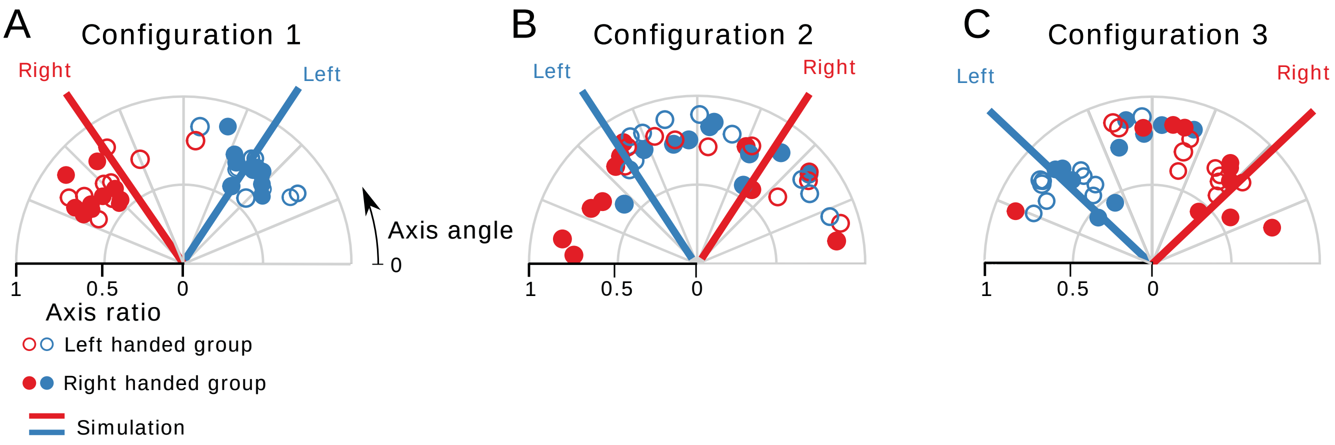
A
Configuration 1
Right
Left
Axis angle
0
1
0.5
0
Axis ratio
○○ Left handed group
●● Right handed group
Simulation
B
Configuration 2
Left
Right
1
0.5
0
C
Configuration 3
Left
Right
1
0.5
0

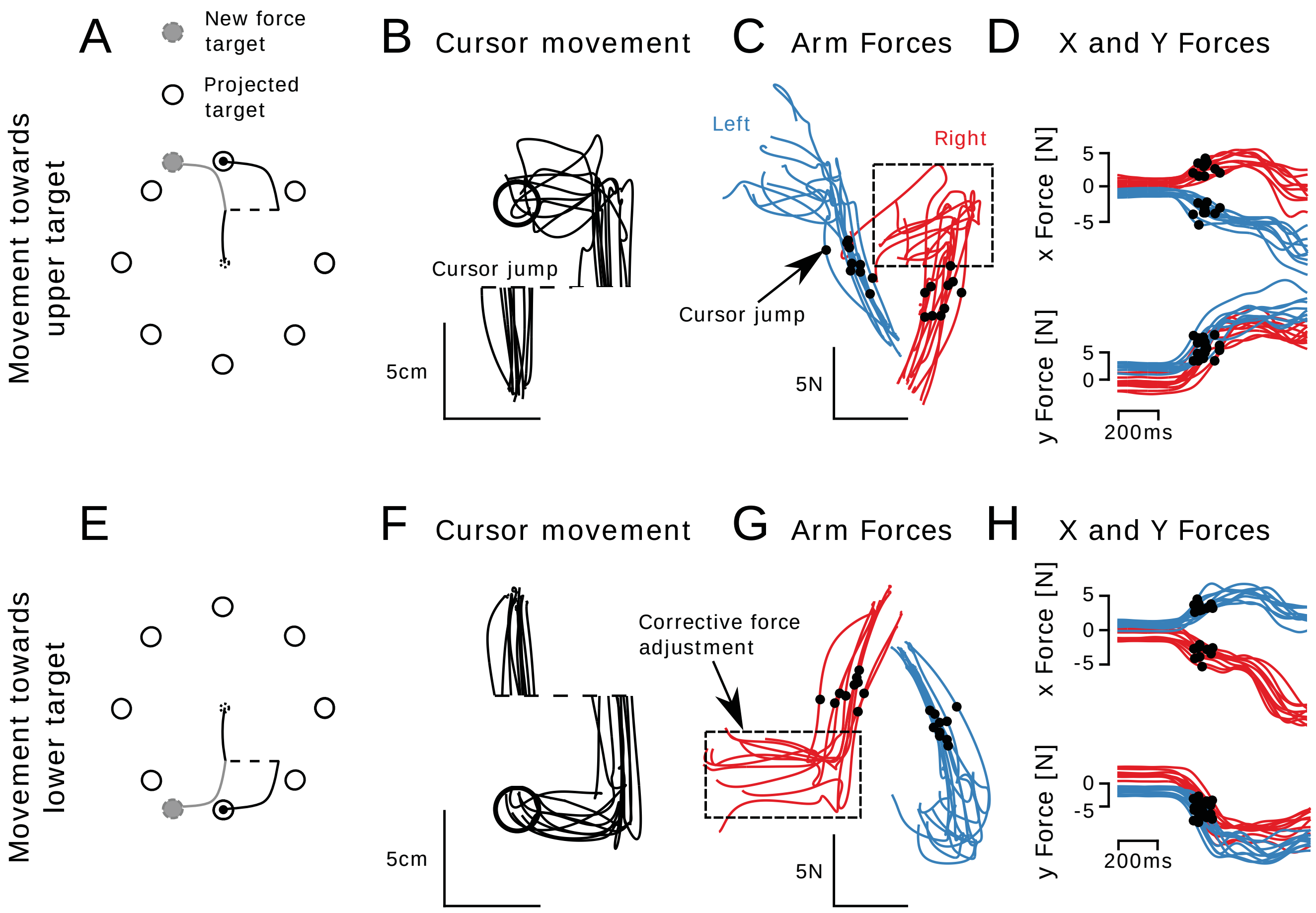
A
New force target
Projected target
Movement towards upper target
B Cursor movement
Cursor jump
5cm
C Arm Forces
Left
Right
Cursor jump
5N
D X and Y Forces
x Force [N]
5
0
-5
y Force [N]
5
0
200ms
E
Movement towards lower target
F Cursor movement
5cm
G Arm Forces
Corrective force adjustment
5N
H X and Y Forces
x Force [N]
5
0
-5
y Force [N]
0
-5
200ms

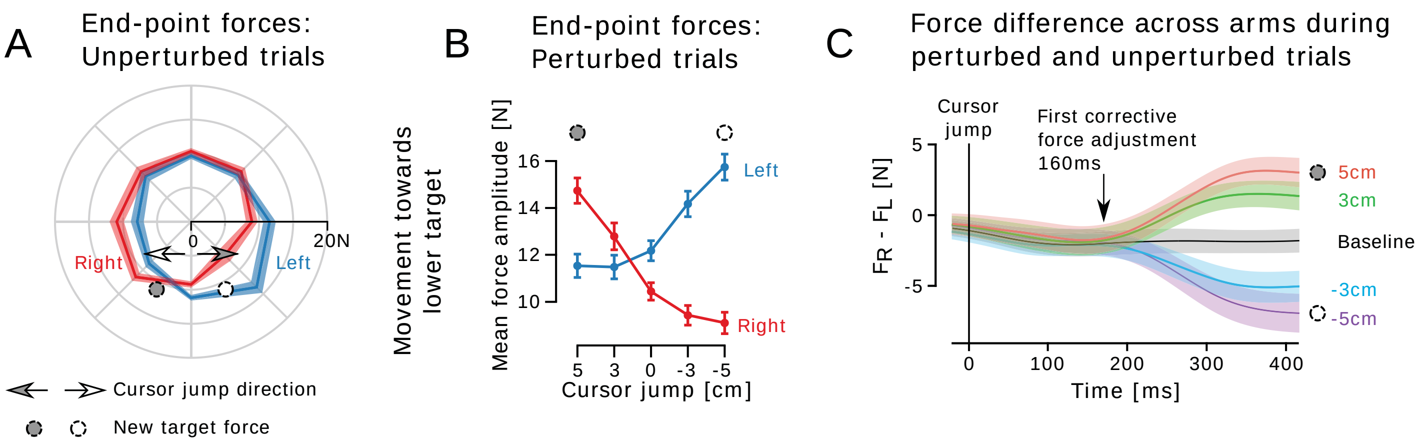

A End-point forces: Unperturbed trials

B End-point forces: Perturbed trials

C Force difference across arms during perturbed and unperturbed trials

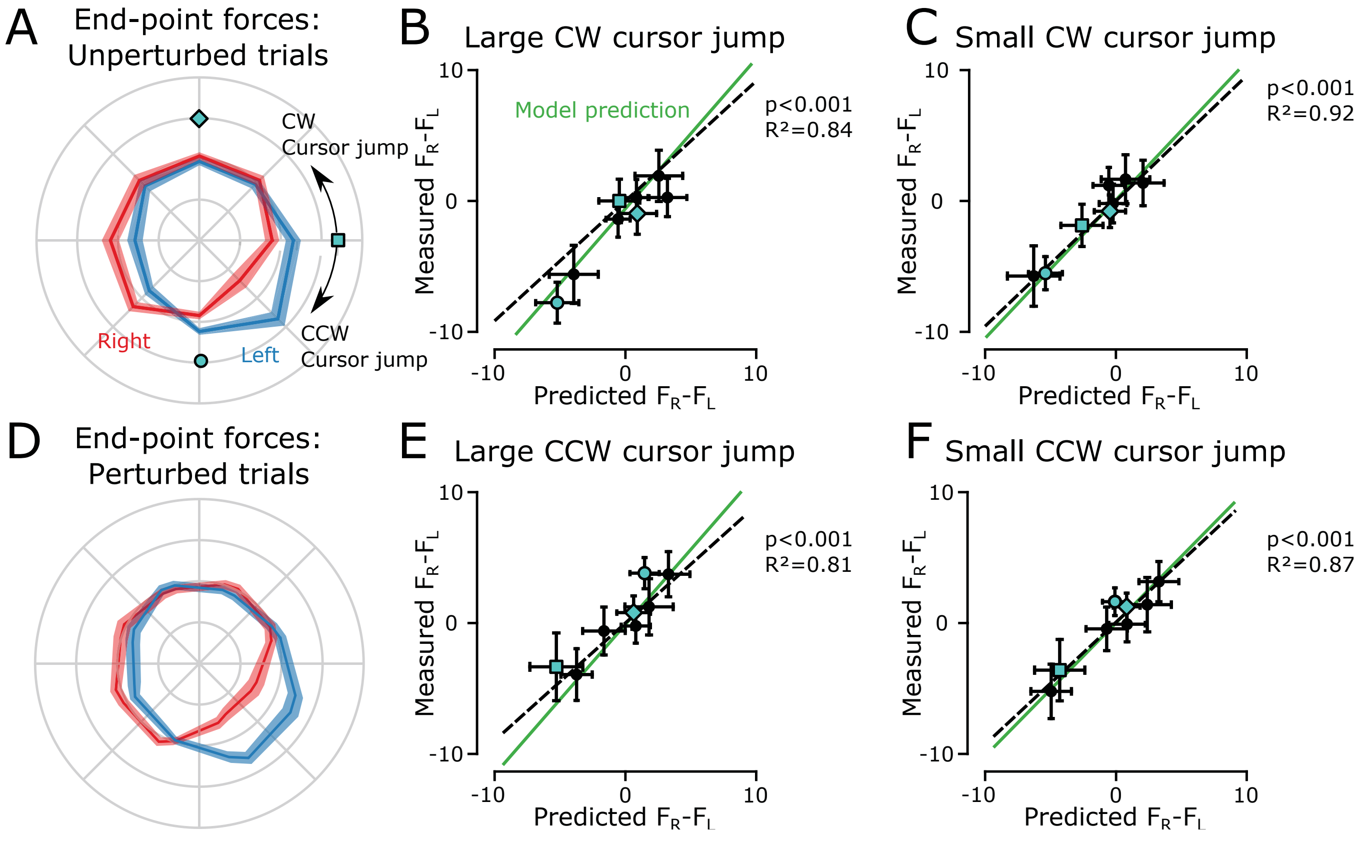
A
End-point forces:
Unperturbed trials
CW
Cursor jump
CCW
Cursor jump
Right
Left
B
Large CW cursor jump
Model prediction
p<0.001
R²=0.84
C
Small CW cursor jump
p<0.001
R²=0.92
D
End-point forces:
Perturbed trials
E
Large CCW cursor jump
p<0.001
R²=0.81
F
Small CCW cursor jump
p<0.001
R²=0.87
Measured F_R-F_L
Predicted F_R-F_L
10
0
-10
-10
0
10

Joint configuration	Shoulder angle (θ_1) [°]	Elbow angle (θ_2) [°]
1	23.86 +- 5.94	88.53 +- 5.08
2	16.53 +- 3.98	76.51 +- 5.70
3	21.28 +- 5.59	51.59 +- 11.26